Biointerface Research in Applied Chemistry
Open-Access Journal (ISSN: 2069-5837)

Article
Volume 14, Issue 5, 2024, 105
https://doi.org/10.33263/BRIAC154.105

Colorimetric Screen-Printed Label Using Low Molecular Weight Chitosan Grafted with Rosolic Acid for pH and Ammonia Gas Sensing

Arnat Ronte [1], Jongjit Chalitangkoon [1,2], Pathavuth Monvisade [1,*]

[1] Polymer Synthesis and Functional Materials Research Unit, Department of Chemistry, School of Science, King Mongkut's Institute of Technology Ladkrabang, Chalongkrung Road, Ladkrabang, Bangkok 10520, Thailand
[2] Department of Chemical and Biological Engineering, BioProducts Institute, University of British Columbia, 2360 East Mall, Vancouver, BC V6T 1Z3, Canada.
* Correspondence: pathavuth.mo@kmitl.ac.th;

Scopus Author ID 18133833400
Received: 25.02.2024; Accepted: 12.05.2024; Published: 21.07.2024

Abstract: Colorimetric sensing technologies are valued for their simplicity and adaptability, yet their large-scale production remains economically challenging. This study presents a cost-effective colorimetric pH sensor developed from low molecular weight chitosan (LC) grafted with rosolic acid (LCRA), engineered as a pH-sensitive colorant for screen-printing inks. LCRA was synthesized *via* a Mannich reaction and characterized using ^{1}H NMR, FT-IR, and UV-Vis spectroscopy. LCRA showed reduced crystallinity and thermal stability alongside notable improvements in water solubility compared to its LC precursor. The LCRA ink displayed compatibility with various substrates, including polypropylene spun bond, filter paper, and cotton, applying easily *via* screen printing without any dye leaching. Notably, it exhibited a responsive color change from orange-yellow to pink-red in response to pH adjustments between 4.0 and 12.0 and upon exposure to ammonia gas. These findings position the LCRA label as a versatile and efficient solution for visual pH detection across various applications.

Keywords: chitosan; polymeric dye; rosolic acid; screen-printing; pH sensor; ammonia sensor.

1. Introduction

In recent years, colorimetric sensor materials have garnered significant attention for their ability to detect a wide array of analytes through visually discernible color changes. This unique capability has led to their widespread application in diverse fields, such as food safety monitoring [1-3], medical diagnostics [4-6], environmental pollution detection [7,8], and safety systems in industrial processes [9,10]. Generally, these sensors are fabricated by incorporating indicator dyes onto natural or synthetic polymers through adsorption [11], entrapment [12,13], and covalent immobilization (grafting) [14,15]. Although adsorption and entrapment offer simplicity, they tend to suffer from poor dye-leaching resistance. Covalent immobilization, on the other hand, acquires dye molecules onto polymers, forming a robust polymeric dye system that minimizes the risk of leaching, thereby offering enhanced stability, biocompatibility, minimal toxicity, and superior color fastness [15,16]. However, this synthesis process's complexity and multi-step nature often increase production time and costs, presenting challenges in achieving efficiency and scalability.

Chitosan (CS), a cationic linear polysaccharide derived from chitin through alkaline deacetylation, stands as a natural biological resource, offering numerous significant advantages, including high biocompatibility, non-toxicity, biodegradability, abundance, and cost-effectiveness. Additionally, it exhibits well-established biological activities like antibacterial and antifungal properties [17,18]. CS comprises glucosamine (GlcN) and N-acetyl glucosamine (GlcNAc) units linked by β-1,4 glycosidic linkage [19]. The existence of hydroxyl and amino groups within its structure facilitates chemical modification, enabling the creation of a diverse array of valuable biopolymers suitable for a wide range of applications. Regarding CS-based polymeric dyes, several organic dyes, such as methyl red and rose bengal [20], sunset yellow and allura red [21], anthraquinone [22], and pyran flavylium-based indicator dyes [23], have been grafted onto CS and its derivatives. However, these approaches still require complicated synthesis and purification steps. In our prior research, a one-pot synthesis Mannich reaction was employed to graft rosolic acid (RA) and phenol red (PR) onto CS, utilizing them as colorants for creating a colorimetric pH-sensing film [24]. These films exhibited various color changes dependent on the pH level while demonstrating exceptional color stability and resistance to dye leaching, ensuring their reliability across various applications. Nevertheless, crosslinking of long-chain CS hindered synthesizing derivatives with higher dye content, particularly with increased formaldehyde levels. This phenomenon resulted in the formation of high-viscosity or insoluble products [25], presenting a significant challenge in producing colorimetric sensors with enhanced intensity from these derivatives.

As the usage of colorimetric sensors continues to escalate, their mass production requires various technologies, such as film extrusion, printing, and coating, to effectively meet the growing demand [26-28]. Among these techniques, screen printing is a prominent printing method that offers advantages in terms of its inherent simplicity, cost-effectiveness, reproducibility, and uniformity [29]. Moreover, its versatility in accommodating intricate designs enhances its appeal across various applications. Therefore, achieving high-definition printing patterns in screen printing requires precise dispersion of colorant and other components within the ink system [30]. Despite the favorable characteristics of polymeric dyes, there is a lack of documentation regarding using CS-based polymeric dyes as colorants in screen-printing ink.

Herein, we present an enhancement in the dye content of CS-based polymeric dyes by utilizing LC-based polymeric dye as a colorant in screen-printing ink. LC-based polymeric dyes in aqueous form show promise because they improve dispersion in water-based ink. This effectively resolves ink dispersion issues while improving the quality of screen-printed sensor labels. The LCRA polymeric dye was synthesized by grafting RA onto the LC *via* the one-pot synthesis Mannich reaction (Scheme 1). The structure of LCRA was characterized using ^{1}H NMR, FT-IR, UV-Vis, and XRD spectroscopy.

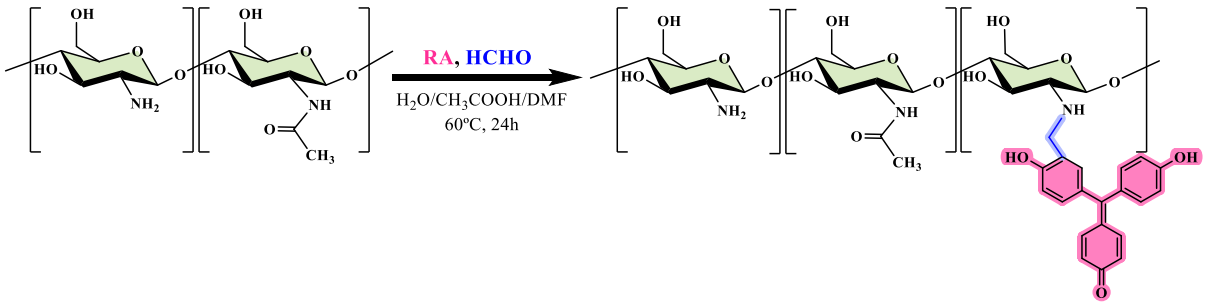

Scheme 1. Synthesis route of LCRA polymeric dye *via* a one-pot Mannich reaction.

Additionally, thermal behavior and pH-dependent water solubility were investigated. The LCRA was then combined with a water-based ink formulation to produce screen-printing ink for the LCRA sensing label. The color response of the printed label to buffer pH solutions and ammonia gas was used to investigate LCRA's sensing properties.

2. Materials and Methods

2.1. Materials.

CS (Degree of deacetylation, DD = 0.92; M.W. ~470 kDa) was purchased from Eland Co., Ltd. RA was purchased from Acros Organic Co. Ltd. Formaldehyde (37% w/w), dimethylformamide, ammonia solution (30% w/w), and hydrogen peroxide (30% w/w) were provided by Carlo Erba (Italy). All other reagents were analytical grade and used without further purification.

2.2. Synthesis of LC.

The LC was synthesized based on a method adapted from previous research [31]. In brief, 8 g CS was completely dissolved in a 320 mL solution of 2% acetic acid. Subsequently, 80 mL of hydrogen peroxide was added dropwise to the solution. The mixture was stirred and allowed to react at 50ºC for 5 h. After the reaction, neutralization was carried out with 2.5 M NaOH, and ethanol was then gradually added with stirring to precipitate the product. The mixture was filtered and washed several times with ethanol. Finally, it was dialyzed against distilled water for 5 days before undergoing freeze-drying to obtain the purified product. The resulting product exhibited a molecular weight of 9.96 ± 0.20 kDa as determined by GPC gel permeation chromatography Nexera Series (Shimadzu, Japan).

2.3. Synthesis of LCRA polymeric dye.

The LCRA was synthesized *via* the Mannich reaction adapted from our previous work [24]. In brief, 1 g LC was dissolved in a 100 mL 1% w/v acetic acid solution. Subsequently, 1.699 g RA dissolved in 50 mL dimethylformamide, and 0.476 g formaldehyde was added to the mixture. The reaction was carried at 60ºC for 24 h. After completion of the reaction, 0.5 M NaOH and ethanol were added to induce precipitation. The resulting mixture was filtered and washed with ethanol several times. The precipitate was then re-precipitated, washed with 70% v/v ethanol/water several times, and dried at 60ºC.

2.4. Structural characterization.

The integration of signals of 1H NMR spectra calculated the degree of substitution (%DS). The spectra of derivatives were detected in the D_2O/CF_3COOH system performed on the JNM-ECZ-500R/S1 spectrometer (JEOL, Japan). The %DS The degree of substitution was calculated from ^1H NMR data:

$$\%DS=(1\text{-}DD)\times\frac{3}{11}\times\frac{H_{Ar}}{H_7}\times100 \qquad (1)$$

where H_{Ar} is the integral area of aromatic protons from δ_H 6.3-7.7 ppm; H_7 is the integral area of protons at C_7.

The FT-IR spectra were recorded using an IRTracer-100 spectrophotometer (Shimadzu, Japan) that scanned from 4000 to 400 cm^{-1} with a 4.0 cm^{-1} resolution. The UV-Vis spectra

were scanned from 200-700 nm using a BlueStar B spectrophotometer (Lab Tech, China). The sample solutions were prepared by dissolving them in a dilute acetic acid solution to obtain a concentration of 0.05% w/v. The crystallinity of the samples was examined according to the XRD recorded at 2θ angles ranging from 5º to 40º, employing a Smartlab SE diffractometer (RIGAKU, Japan). The thermal behavior of the samples was analyzed using the thermogravimetric analysis (TGA) instrument TGA/DSC 3+ STARe System (Mettler-Toledo, Switzerland) at a temperature ranging from 30 to 800ºC with a heating rate of 10ºC/min under N_2 atmosphere. The water-solubility was estimated by turbidity assay. 25 mg of the samples were dissolved in 25 mL of 0.1 M HCl, and the pH was adjusted with NaOH solution. Turbidity was measured by recording the transmittance at 660 nm with a UV-Vis spectrophotometer.

2.5. Preparation of LCRA label.

To create the label, LCRA polymeric dye was dissolved in a 1% w/v acetic acid solution, resulting in a 1% w/v LCRA solution. Subsequently, 20 g of this solution was mixed with 50 g of water-based ink (with a viscosity of approximately 17000 mPa.s) using an IKA RW 20 mechanical stirrer (Germany). After obtaining the ink, the LCRA label was prepared by screen-printing it onto a substrate, including polypropylene spun bond, filter paper, and cotton. The printed label was subsequently dried using an electric hair dryer and stored in a desiccator for a week before testing.

2.6. Dye leaching test.

The leaching resistance of the printed label was evaluated by immersing a 2×2 cm sample in various solvents: 10 mL of 10%, 50%, and 95% ethanol/water solutions, as well as DI water, at room temperature for 24 h. Subsequently, UV–Vis spectra of the immersed solutions were recorded using a UV-Vis spectrophotometer within the range of 300 to 600 nm.

2.7. Color measurement.

The color response of the sensing label at different buffer pH levels was evaluated through a HunterLab MiniScan XE Plus colorimeter (HunterLab Associates, USA). The label with a size of 2×2 cm was immersed in buffer solutions with pH values ranging from 4.0 to 12.0 for 10 min. The color parameters were determined in the CIELab color space. The total color difference (*ΔE*) was calculated using the following equation:

$$\Delta E = \sqrt{(\Delta L)^2 + (\Delta a)^2 + (\Delta b)^2} \qquad (2)$$

where ΔL is the difference in lightness-darkness, Δa is the difference in redness-greenness, and Δb is the difference in yellowness-blueness.

2.8. Ammonia sensing test.

To evaluate the responsiveness of the label to ammonia, a 2×2 cm label was affixed to the inner surface of a testing chamber measuring 8.1×8.1×8.4 cm. Subsequently, 10 mL of ammonium hydroxide solution with concentrations of 0.075%, 0.15%, 0.30%, and 0.45% v/v was introduced into the test chamber. A colorimeter was used to record the color change at 3-minute intervals over a 30-minute period.

3. Results and Discussion

3.1. Structural characterization.

The ^{1}H NMR spectra of CS, LC, and LCRA are illustrated in Figure 1a. The CS spectra displayed a peak at 2.9-3.2 ppm corresponding to H_2 of GlcN units. Peaks between the 3.3-4.1 ppm range were attributed to H_3-H_6 and $H_{2'}$-$H_{6'}$. A peak at 1.9-2.0 ppm was also assigned to H_7 of GlcNAc units [32]. Similar to CS, the LC spectra indicated preserving its primary monomeric structure after depolymerization. After the grafting process, the LCRA spectra revealed a new peak in the region of 6.3-7.7 ppm, assigned to the aromatic proton of RA, confirming the presence of RA in LC. The %DS of LCRA calculated from the ^{1}H NMR spectra was 14%.

The FT-IR spectra of CS, LC, LCRA, and pristine RA are shown in Figure 1b. The characteristic chitosan pattern was observed in CS, LC, and LCRA spectra: C=O stretching (amide I) at 1656 cm^{-1}, N–H bending of the primary amine at 1597 cm^{-1}, and C–N stretching (amide III) at 1323 cm^{-1} [33]. In addition, a vibration signal corresponding to C=C stretching in the aromatic ring of RA can be observed in the LCRA spectrum at 1571 cm^{-1}, which shifted from the pristine RA at 1581 cm^{-1}. This result suggests that RA has been successfully grafted onto the LC backbone.

The UV-Vis spectra of LC, LCRA, and LC mixed with RA are displayed in Figure 1c. The spectrum of LC did not show any absorption peak in the 400-500 nm range. In the case of LCRA, an absorption peak was observed at 484 nm, while LC mixed with RA observed an absorption peak at 475 nm, corresponding to the characteristic absorption of RA. This finding corresponds with the bathochromic shift caused by the covalent connection between LC and the RA ring, indicating successful grafting of RA onto the LC [24].

The XRD pattern of CS, LC, and LCRA were displayed in Figure 1d. The diffraction spectrum of CS exhibited three peaks at 2θ values of 10.5º, 19.9º, and 22.7º, corresponding to the reflection planes 020, 200, and 220 of CS in the hydrated form, respectively [34,35]. In the case of LC, a pattern resembling that of CS was noted, but with an enhanced peak intensity at 2θ = 19.9º. This increase can be attributed to the recrystallization of a shorter chain LC [36,37]. After the grafting process, LCRA displayed a substantial decrease in crystallinity due to the incorporation of the RA group, resulting in a significant weakening of hydrogen bonds within the LC chain. This observation provides additional evidence confirming the successful grafting of RA onto LC.

The thermal behavior of CS, LC, and LCRA was investigated using TGA, as displayed in Figure 1e. Both CS and LC exhibited two stages of weight loss in their TGA and DTG curves. The initial stage, occurring from 40 to 150ºC, was attributed to the dehydration of absorbed water within the carbohydrate chains [38]. The subsequent stage, occurring from 200 to 400ºC, exhibited a maximum thermal decomposition temperature (T_{max}) of 305 and 289ºC for CS and LC, respectively, attributed to polymer chain depolymerization and decomposition [39]. The thermal stability of LC appeared slightly lower than that of CS, attributed to its reduced molecular weight [40,41]. In comparison to LC, LCRA exhibited three stages of weight loss. The first stage of weight loss occurred from 40 to 140ºC due to the loss of absorbed water. The second and third stages occurred between 175 to 550ºC, attributed to the decomposition of the LCRA chain. DTG analysis revealed a T_{max} at 278ºC, suggesting a decrease in the thermal stability of LCRA. This result can be attributed to the introduction of the RA group hindering the packing of LC chains, resulting in a decline in thermal stability.

The pH-dependent water solubility of CS, LC, and LCRA are shown in Figure 1f. In the CS solution, the transmittance approached near 100% under low pH conditions while CS remained in a dissolved state. A significant rise in solution turbidity was observed when pH > 6.8, resulting from the deprotonation of $–NH_3^+$ groups to $–NH_2$ groups, indicating the formation of an insoluble phase. Compared to CS, the initial turbidity of the LC solution shifted to pH 7.6. This shift can be ascribed to the reduction in intermolecular interactions, such as hydrogen bonding and hydrophobic interactions, resulting from the decreased molecular weight [41,42]. In the case of LCRA, the transmittance remained above 85% at pH 2.0-5.0, indicating good solubility. However, a dramatic decrease in transmittance was observed when the pH exceeded 6.0, reaching its lowest point at pH 9.0. This phenomenon can be explained by partial crosslinking between LCRA chains resulting from the Mannich reaction [43]. At pH levels exceeding 10.0, there was a notable increase in transmittance, surpassing 80% when the pH reached 12.00, indicating the solubilization of LCRA in alkaline conditions. This finding can be explained by the prevalence of RA in its dianion state (RA^{2-}) when the pH exceeds 10.0 [44]. This transformation leads to electrostatic repulsion between the LCRA chain and enhanced solubility.

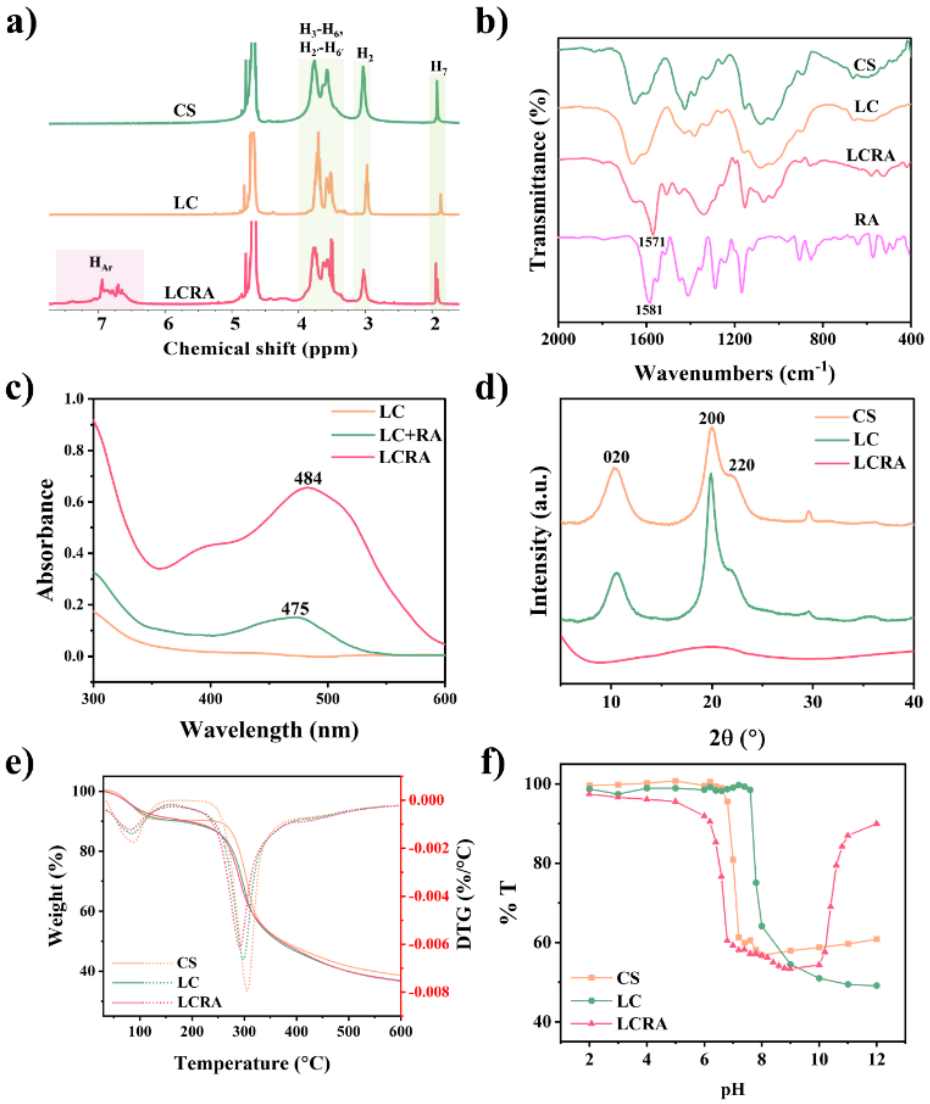

Figure 1. Structural characterization: (**a**) ^{1}H NMR spectra of CS, LC and LCRA; (**b**) FT-IR spectra of CS, LC, and LCRA and RA; (**c**) UV-Vis spectra of LC, LCRA, and LC mixed with RA; (**d**) XRD patterns of CS, LC and LCRA; (**e**) TGA and DTG thermograms of CS, LC, and LCRA; (**f**) pH dependence of solubility of CS, LC, and LCRA.

3.2. Preparation of LCRA inks and application on substrate.

The procedure for creating the LCRA label is illustrated in Figure 2a. Initially, the LCRA polymeric dye solution was blended with water-based ink to obtain the LCRA ink, which was then applied on substrates *via* screen printing to create the LCRA label. Throughout this process, the LCRA polymeric dye is consistently dispersed within the ink, resulting in a homogeneous mixture free of visible particles. Moreover, as evidenced by optical micrographs in Figure 2b, the ink exhibited remarkable versatility in adhering to a range of substrates, including polypropylene spun bond, filter paper, and cotton. This versatility enabled the resultant label to be printed with high-resolution designs, boasting exceptional clarity and showcasing its adaptability and quality across diverse materials.

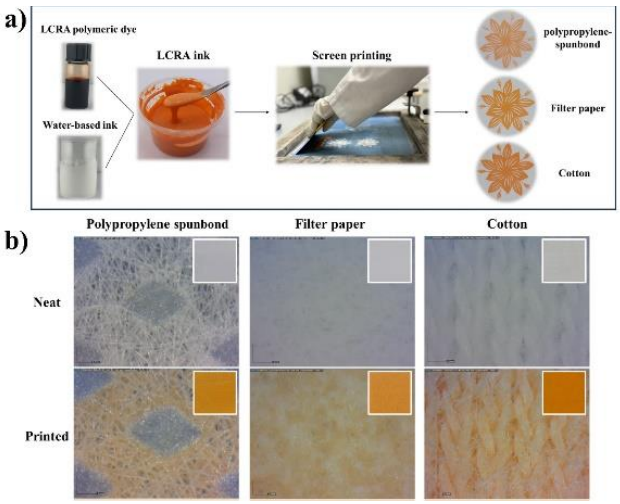

Figure 2. (**a**) Preparation process of the LCRA label; (**b**) optical micrograph of neat and printed on different substrates.

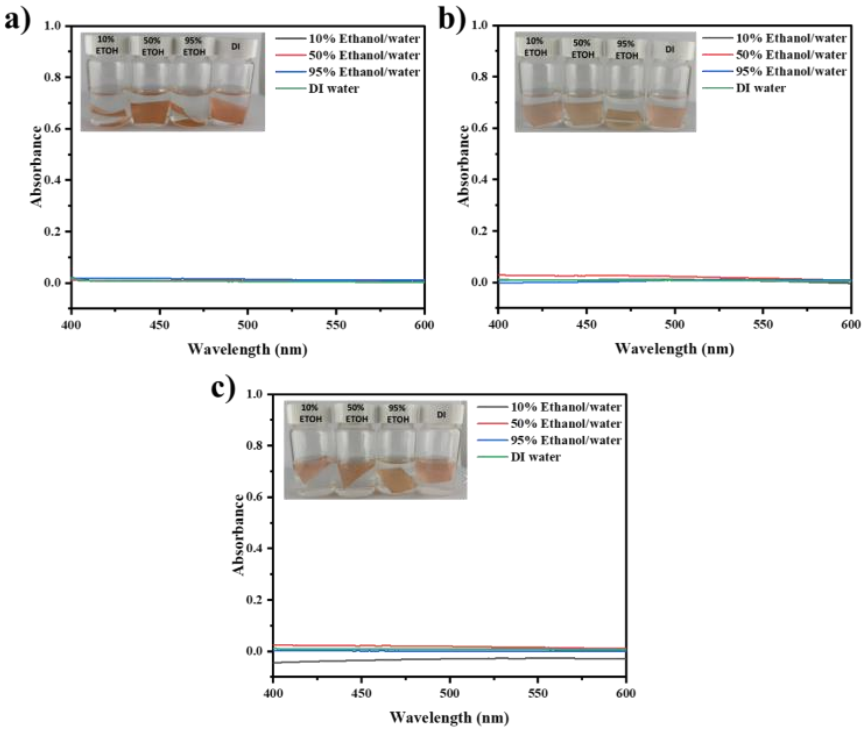

Figure 3. The UV–Vis absorption of solutions wherein LCRA coated on **(a)** cotton; **(b)** filter paper; **(c)** polypropylene spun bond were immersed for 24 h.

3.3. Dye leaching-resistance property.

The dye leaching-resistance property of the LCRA printed on various substrates underwent testing by immersion in 10%, 50%, and 95% ethanol/water, as well as DI water, and the results were illustrated in Figure 3. The UV–Vis spectra of the immersed solutions did not exhibit the characteristic absorption band of the RA, suggesting no leaching of the dye. This observation indicates that establishing covalent bonds between the RA and the polymer effectively mitigates leaching within the LCRA label, thereby enhancing its color fastness and ensuring safety in practical applications.

3.4. pH sensing of LCRA label.

The color change responsiveness of the LCRA printed on the cotton label to different buffer pH solutions was demonstrated in Figure 4. As illustrated in Figure 4a, the color of the label transitioned from orange-yellow to orange-red across the pH range of 4.0–8.0, as observed in the change of color parameter (Figure 4b), with an increase in the *a* value from 26.71 to 41.17, accompanied by a decrease in the *b* value from 22.04 to 9.57. As the pH increased from 8.0 to 12.0, the red hue became significantly more dominant, as evidenced by the rise in the *a* value to 48.12, while simultaneously, the *b* value decreased to below zero. Additionally, in Figure 4c, the *ΔE* values for the label immersed in pH buffers ranging from 6.0 to 12.0 are greater than 5.0, indicating a substantial color difference that is readily noticeable to the naked eye within this pH range [45]. The color change of the LCRA label is attributed to resonance transformation in the RA chemical structure, wherein RA converts from H_2RA (yellow) in acidic conditions to RA^{2-} (red) in neutral or alkaline conditions [44]. The above results demonstrate that the LCRA label exhibits remarkable sensitivity across a wide pH range, indicating significant potential for sensing applications.

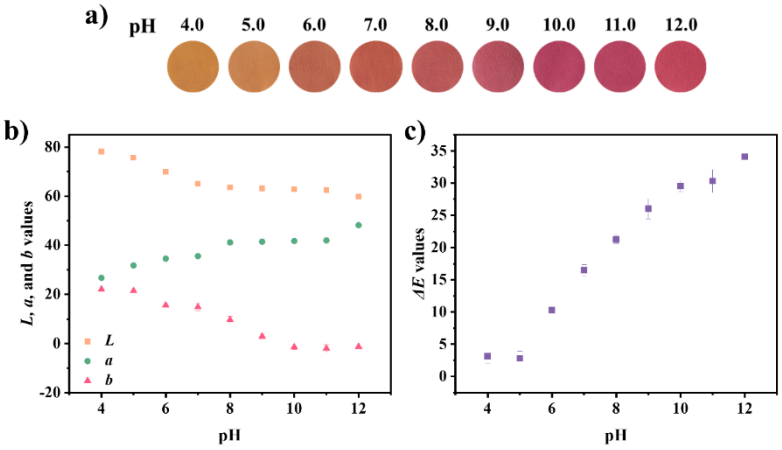

Figure 4. (**a**) The optical color change; (**b**) *L*, *a*, and *b* values; (**c**) *ΔE* values of LCRA printed on cotton label after immersed in buffer solutions pH 4.0-12.0.

3.5. Ammonia sensing of LCRA label.

The color response of LCRA printed on a cotton label when exposed to ammonia, generated from ammonium hydroxide solutions with concentrations of 0.075%, 0.15%, 0.30%, and 0.45% v/v for 30 minutes, is illustrated in Figure 5. As depicted in Figure 5a, after 15 minutes of ammonia exposure, the label underwent noticeable color changes over time, transitioning from orange-yellow to pink-red. Moreover, the intensity of the blue hue increased with both reaction time and ammonia concentrations, as evidenced by the decreasing *b* values

(Figure 5b). Furthermore, the *ΔE* values (depicted in Figure 5c) indicated a noticeable alteration in the label's color within the initial 3 minutes, with values exceeding 5.0 even at the lowest test concentration. The color responsiveness ability of the label can be explained by the reaction of ammonia with water molecules, leading to the formation of ammonium hydroxide, which subsequently dissociates into ammonium ion (NH_4^+) and hydroxide ion (OH^-). The presence of OH^- triggers the deprotonation of RA molecules, ultimately causing the label's color change [46]. This result suggests that the LCRA label can effectively serve as a colorimetric sensor for detecting and monitoring ammonia levels, making it a promising candidate for applications in environmental monitoring, food safety, and industrial processes where ammonia detection is critical.

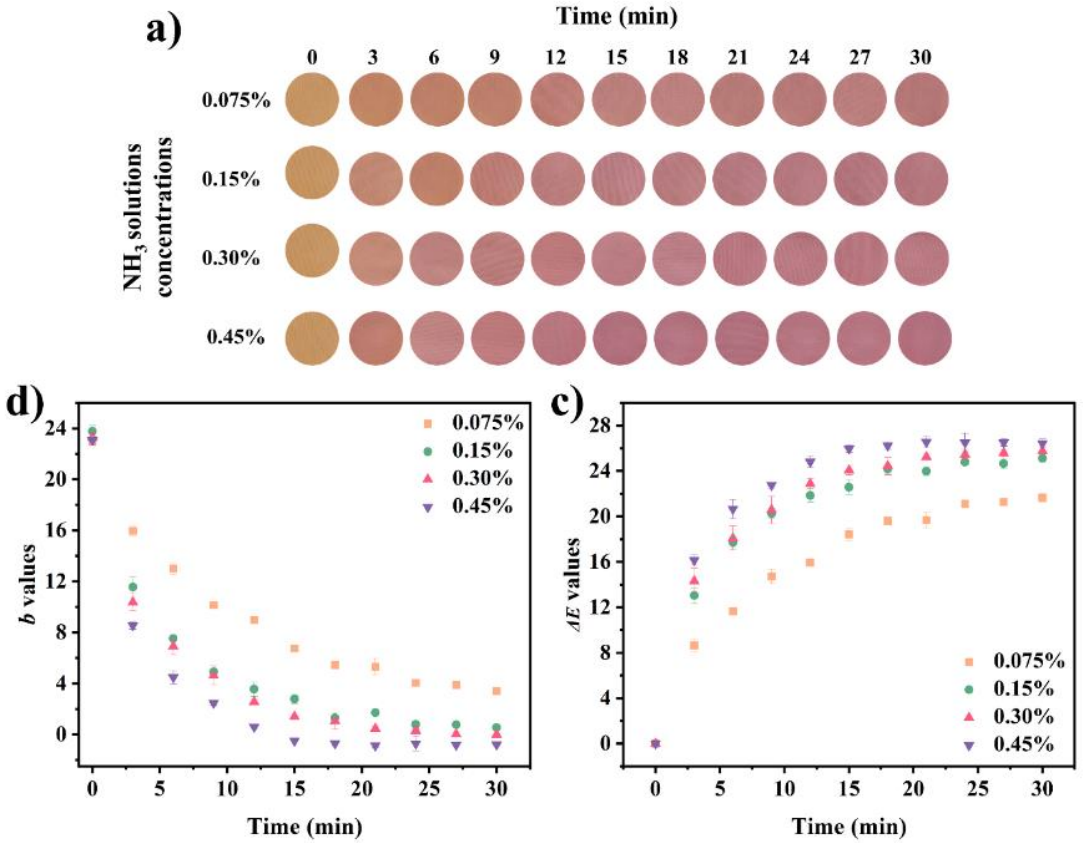

Figure 5. (**a**) The optical color change; (**b**) *b* values; (**c**) *ΔE* values of LCRA printed on cotton label exposed to ammonia produced by ammonium hydroxide solution at concentrations of 0.075%, 0.15%, 0.30%, and 0.45% v/v.

4. Conclusions

In conclusion, our research has successfully created a screen-printed label capable of responding to pH changes, utilizing the LCRA polymeric dye. The synthesis of LCRA, conducted through a Mannich reaction, was rigorously confirmed using ^{1}H NMR, FT-IR, and UV-Vis spectroscopy. By choosing low molecular weight chitosan (LC) over neat chitosan, we significantly increased the dye content to 14%, improved the solubility in alkaline conditions (pH > 10.0), and reduced crystallinity. These enhancements made the LCRA ink exceptionally fit for high-definition printing across various materials, ensuring no dye leakage. Notably, the LCRA labels demonstrated acute sensitivity to pH levels ranging from 4.0 to 12.0 and to ammonia gas, showing clear color transitions from orange-yellow to pink-red. This breakthrough highlights the immense potential of LCRA labels as versatile sensors for visually

detecting pH levels and alkaline gases, offering broad applicability in diverse colorimetric sensing applications.

Funding

This research was funded by the National Science, Research and Innovation Fund (NSRF) (Grant number RE-KRIS/FF66/55), School of Science, King Mongkut's Institute of Technology Ladkrabang, Thailand (Grant No. RA/TA-2564-M003), and the Royal Golden Jubilee Program (RGJ: grant No. PHD/0080/2559).

Acknowledgments

The authors would like to thank the Scientific Instruments Center, School of Science, King Mongkut's Institute of Technology Ladkrabang for ^{1}H NMR and XRD testing.

Conflicts of Interest

The authors declare no conflict of interest.

References

1. de Azevedo, E.S.; Noreña, C.P.Z. Anthocyanin-based indicators design by polyelectrolyte complexation: A study on structural and thermodynamic properties, and application for milk freshness assessment. *Food Hydrocoll.* **2024**, *147*, 109389, https://doi.org/10.1016/j.foodhyd.2023.109389.
2. Miao, Y.; Chen, Z.; Zhang, J.; Li, N.; Wei, Z.; Zhang, Y.; Wu, X.; Liu, J.; Gao, Q.; Sun, X.; Sun, Q.; Zhang, J. Exopolysaccharide riclin and anthocyanin-based composite colorimetric indicator film for food freshness monitoring. *Carbohydr. Polym.* **2023**, *314*, 120882, https://doi.org/10.1016/j.carbpol.2023.120882.
3. Jia, X.; Ma, P.; Tarwa, K.; Mao, Y.; Wang, Q. Development of a novel colorimetric sensor array based on oxidized chitin nanocrystals and deep learning for monitoring beef freshness. *Sens. Actuators B: Chem.* **2023**, *390*, 133931, https://doi.org/10.1016/j.snb.2023.133931.
4. Lee, T.; Kim, I.; Cheong, D.Y.; Roh, S.; Jung, H.G.; Lee, S.W.; Kim, H.S.; Yoon, D.S.; Hong, Y.; Lee, G. Selective colorimetric urine glucose detection by paper sensor functionalized with polyaniline nanoparticles and cell membrane. *Anal. Chim. Acta* **2021**, *1158*, 338387, https://doi.org/10.1016/j.aca.2021.338387.
5. Carneiro, M.C.C.G.; Rodrigues, L.R.; Moreira, F.T.C.; Sales, M.G.F. Colorimetric Paper-Based Sensors against Cancer Biomarkers. *Sensors* **2022**, *22*, 3221, https://doi.org/10.3390/s22093221.
6. Sakboriboon, Y.; Chalitangkoon, J.; Monvisade, P. Improving the Fluorescence of Carbon Dots Through Boron and Silver Doping: A Single-Step Microwave Synthesis Approach. **2024**, *14*, 44, https://doi.org/10.33263/BRIAC142.044.
7. Cho, Y.B.; Jeong, S.H.; Chun, H.; Kim, Y.S. Selective colorimetric detection of dissolved ammonia in water via modified Berthelot's reaction on porous paper. *Sens. Actuators B: Chem.* **2018**, *256*, 167-175, https://doi.org/10.1016/j.snb.2017.10.069.
8. Rasheed, T.; Shafi, S.; Ali, J.; Sher, F.; Rizwan, K.; Khan, S. Recent advances in chemically and biologically synthesized nanostructures for colorimetric detection of heavy metal. *J. King Saud Univ. Sci.* **2022**, *34*, 101745, https://doi.org/10.1016/j.jksus.2021.101745.
9. Park, Y.K.; Oh, H.J.; Bae, J.H.; Lim, J.Y.; Lee, H.D.; Hong, S.I.; Son, H.S.; Kim, J.H.; Lim, S.J.; Lee, W. Colorimetric Textile Sensor for the Simultaneous Detection of NH_3 and HCl Gases. *Polymers* **2020**, *12*, 2595, https://doi.org/10.3390/polym12112595.
10. Lee, S.; Lee, E.-H.; Lee, S.-W. A Flexible and Attachable Colorimetric Film Sensor for the Detection of Gaseous Ammonia. *Biosensors* **2022**, *12*, 664, https://doi.org/10.3390/bios12080664.
11. Guo, M.; Wang, H.; Wang, Q.; Chen, M.; Li, L.; Li, X.; Jiang, S. Intelligent double-layer fiber mats with high colorimetric response sensitivity for food freshness monitoring and preservation. *Food Hydrocoll.* **2020**, *101*, 105468, https://doi.org/10.1016/j.foodhyd.2019.105468.

12. Liu, D.; Cui, Z.; Shang, M.; Zhong, Y. A colorimetric film based on polyvinyl alcohol/sodium carboxymethyl cellulose incorporated with red cabbage anthocyanin for monitoring pork freshness. *Food Packag. Shelf Life* **2021**, *28*, 100641, https://doi.org/10.1016/j.fpsl.2021.100641.
13. Nadi, M.; Razavi, S.M.A.; Shahrampour, D. Fabrication of green colorimetric smart packaging based on basil seed gum/chitosan/red cabbage anthocyanin for real-time monitoring of fish freshness. *Food Sci. Nutr.* **2023**, *11*, 6360-6375, https://doi.org/10.1002/fsn3.3574.
14. Khanjanzadeh, H.; Park, B.-D. Covalent immobilization of bromocresol purple on cellulose nanocrystals for use in pH-responsive indicator films. *Carbohydr. Polym.* **2021**, *273*, 118550, https://doi.org/10.1016/j.carbpol.2021.118550.
15. Zhou, J.; Jiang, B.; Gao, C.; Zhu, K.; Xu, W.; Song, D. Stable, reusable, and rapid response smart pH-responsive cotton fabric based on covalently immobilized with naphthalimide-rhodamine probe. *Sens. Actuators B: Chem.* **2022**, *355*, 131310, https://doi.org/10.1016/j.snb.2021.131310.
16. Mao, H.; Wang, C.; Wang, Y. Synthesis of polymeric dyes based on waterborne polyurethane for improved color stability. *New J. Chem.* **2015**, *39*, 3543-3550, https://doi.org/10.1039/C4NJ02222J.
17. Flórez, M.; Guerra-Rodríguez, E.; Cazón, P.; Vázquez, M. Chitosan for food packaging: Recent advances in active and intelligent films. *Food Hydrocoll.* **2022**, *124*, 107328, https://doi.org/10.1016/j.foodhyd.2021.107328.
18. Islam, S.; Rahman Bhuiyan, M.A.; Islam, M.N. Chitin and Chitosan: Structure, Properties and Applications in Biomedical Engineering. *J. Polym. Environ.* **2017**, *25*, 854-866, https://doi.org/10.1007/s10924-016-0865-5.
19. Muxika, A.; Etxabide, A.; Uranga, J.; Guerrero, P.; de la Caba, K. Chitosan as a bioactive polymer: Processing, properties and applications. *Int. J. Biol. Macromol.* **2017**, *105*, 1358-1368, https://doi.org/10.1016/j.ijbiomac.2017.07.087.
20. Schoolaert, E.; Steyaert, I.; Vancoillie, G.; Geltmeyer, J.; Lava, K.; Hoogenboom, R.; De Clerck, K. Blend electrospinning of dye-functionalized chitosan and poly(ε-caprolactone): towards biocompatible pH-sensors. *J. Mater. Chem. B* **2016**, *4*, 4507-4516, https://doi.org/10.1039/C6TB00639F.
21. Lv, D.; Zhang, M.; Cui, J.; Li, W.; Zhu, G. A Novel Preparation Method of Two Polymer Dyes with Low Cytotoxicity. *Materials* **2017**, *10*, 219, https://doi.org/10.3390/ma10030219.
22. Lv, D.; Cui, J.; Wang, Y.; Zhu, G.; Zhang, M.; Li, X. Synthesis and color properties of novel polymeric dyes based on grafting of anthraquinone derivatives onto *O*-carboxymethyl chitosan. *RSC Adv.* **2017**, *7*, 33494-33501, https://doi.org/10.1039/C7RA04024E.
23. Pires, A.S.; Gomes, V.; Neves, D.; Mateus, N.; de Freitas, V.; Cruz, L. Colorimetric pH-Responsive Biomaterials Based on Pyranoflavylium-Biopolymer Hybrid Conjugates. *ACS Appl. Polym. Mater.* **2022**, *4*, 4961-4971, https://doi.org/10.1021/acsapm.2c00514.
24. Chalitangkoon, J.; Monvisade, P. Synthesis of chitosan-based polymeric dyes as colorimetric pH-sensing materials: Potential for food and biomedical applications. *Carbohydr. Polym.* **2021**, *260*, 117836, https://doi.org/10.1016/j.carbpol.2021.117836.
25. Chalitangkoon, J.; Monvisade, P. Dual pH/thermal-dependent coloring polymeric dye through Mannich reaction of chitosan: Synthesis and characterization. *Carbohydr. Polym.* **2019**, *223*, 115049, https://doi.org/10.1016/j.carbpol.2019.115049.
26. Zhai, X.; Wang, X.; Zhang, J.; Yang, Z.; Sun, Y.; Li, Z.; Huang, X.; Holmes, M.; Gong, Y.; Povey, M.; Shi, J.; Zou, X. Extruded low density polyethylene-curcumin film: A hydrophobic ammonia sensor for intelligent food packaging. *Food Pack. Shelf Life* **2020**, *26*, 100595, https://doi.org/10.1016/j.fpsl.2020.100595.
27. Sun, Y.; Wen, J.; Chen, Z.; Qiu, S.; Wang, Y.; Yin, E.; Li, H.; Liu, X. Non-destructive and Rapid Method for Monitoring Fish Freshness of Grass Carp Based on Printable Colorimetric Paper Sensor in Modified Atmosphere Packaging. *Food Anal. Methods* **2022**, *15*, 792-802, https://doi.org/10.1007/s12161-021-02158-2.
28. Alkasir, R.S.J.; Ornatska, M.; Andreescu, S. Colorimetric Paper Bioassay for the Detection of Phenolic Compounds. *Anal. Chem.* **2012**, *84*, 9729-9737, https://doi.org/10.1021/ac301110d.
29. Wang, L.; Wu, Z.; Cao, C. Technologies and Fabrication of Intelligent Packaging for Perishable Products. *Appl. Sci.* **2019**, *9*, 4858, https://doi.org/10.3390/app9224858.
30. Cai, S.; Song, G.; Zhang, G.; Wang, L.; Jian, T.; Xu, J.; Su, F.; Tian, Y. A multicolor fluorescent sensor array based on curcumin and its analogs as a shrimp freshness indicator. *Sens. Actuators B: Chem.***2022**, *367*, 132153, https://doi.org/10.1016/j.snb.2022.132153.

31. Kaemkit, C.; Monvisade, P.; Siriphannon, P.; Nukeaw, J. Water-soluble chitosan intercalated montmorillonite nanocomposites for removal of basic blue 66 and basic yellow 1 from aqueous solution. *J. Appl. Polym. Sci.* **2013**, *128*, 879-887, https://doi.org/10.1002/app.38255.
32. Kasaai, M.R. Determination of the degree of *N*-acetylation for chitin and chitosan by various NMR spectroscopy techniques: A review. *Carbohydr. Polym.* **2010**, *79*, 801-810, https://doi.org/10.1016/j.carbpol.2009.10.051.
33. Liu, J.; Wen, X.-y.; Lu, J.-f.; Kan, J.; Jin, C.-h. Free radical mediated grafting of chitosan with caffeic and ferulic acids: Structures and antioxidant activity. *Int. J. Biol. Macromol.* **2014**, *65*, 97-106, https://doi.org/10.1016/j.ijbiomac.2014.01.021.
34. Podgorbunskikh, E.; Kuskov, T.; Rychkov, D.; Lomovskii, O.; Bychkov, A. Mechanical Amorphization of Chitosan with Different Molecular Weights. *Polymers* **2022**, *14*, 4438, https://doi.org/10.3390/polym14204438.
35. Baklagina, Y.G.; Klechkovskaya, V.V.; Kononova, S.V.; Petrova, V.A.; Poshina, D.N.; Orekhov, A.S.; Skorik, Y.A. Polymorphic Modifications of Chitosan. *Crystallogr. Rep.* **2018**, *63*, 303-313, https://doi.org/10.1134/S1063774518030033.
36. Qin, C.; Du, Y.; Zong, L.; Zeng, F.; Liu, Y.; Zhou, B. Effect of hemicellulase on the molecular weight and structure of chitosan. *Polym. Degrad. Stab.* **2003**, *80*, 435-441, https://doi.org/10.1016/S0141-3910(03)00027-2.
37. Li, J.; Du, Y.; Yang, J.; Feng, T.; Li, A.; Chen, P. Preparation and characterisation of low molecular weight chitosan and chito-oligomers by a commercial enzyme. *Polym. Degrad. Stab.* **2005**, *87*, 441-448, https://doi.org/10.1016/j.polymdegradstab.2004.09.008.
38. Zeng, L.; Qin, C.; Wang, L.; Li, W. Volatile compounds formed from the pyrolysis of chitosan. *Carbohydr. Polym.* **2011**, *83*, 1553-1557, https://doi.org/10.1016/j.carbpol.2010.10.007.
39. Islam, M.M.; Islam, R.; Mahmudul Hassan, S.M.; Karim, M.R.; Rahman, M.M.; Rahman, S.; Nur Hossain, M.; Islam, D.; Aftab Ali Shaikh, M.; Georghiou, P.E. Carboxymethyl chitin and chitosan derivatives: Synthesis, characterization and antibacterial activity. *Carbohydr. Polym. Technol. Appl.* **2023**, *5*, 100283, https://doi.org/10.1016/j.carpta.2023.100283.
40. Jafari, H.; Delporte, C.; Bernaerts, K.V.; De Leener, G.; Luhmer, M.; Nie, L.; Shavandi, A. Development of marine oligosaccharides for potential wound healing biomaterials engineering. *Chem. Eng. J. Adv.* **2021**, *7*, 100113, https://doi.org/10.1016/j.ceja.2021.100113.
41. Tian, M.; Tan, H.; Li, H.; You, C. Molecular weight dependence of structure and properties of chitosan oligomers. *RSC Adv.* **2015**, *5*, 69445-69452, https://doi.org/10.1039/C5RA08358C.
42. Nguyen, T.H.P.; Le, N.A.T.; Tran, P.T.; Bui, D.D.; Nguyen, Q.H. Preparation of water-soluble chitosan oligosaccharides by oxidative hydrolysis of chitosan powder with hydrogen peroxide. *Heliyon* **2023**, *9*, e19565, https://doi.org/10.1016/j.heliyon.2023.e19565.
43. Chalitangkoon, J.; Ronte, A.; Monvisade, P. Carboxyethylation of chitosan-based polymeric dyes for potential pH-sensing applications. *J. Taiwan Inst. Chem. Eng.* **2023**, *149*, 105001, https://doi.org/10.1016/j.jtice.2023.105001.
44. Shokrollahi, A.; Gohari, M.; Ebrahimi, F. Determination of Acidity Constants of p-Rosolic acid and Bromoxylenol Blue by Solution Scanometric Method. *Anal. Bioanal. Chem. Res.* **2018**, *5*, 67-79, https://doi.org/10.22036/ABCR.2017.89026.1153.
45. Prietto, L.; Mirapalhete, T.C.; Pinto, V.Z.; Hoffmann, J.F.; Vanier, N.L.; Lim, L.-T.; Guerra Dias, A.R.; da Rosa Zavareze, E. pH-sensitive films containing anthocyanins extracted from black bean seed coat and red cabbage. *LWT* **2017**, *80*, 492-500, https://doi.org/10.1016/j.lwt.2017.03.006.
46. Bao, Y.; Cui, H.; Tian, J.; Ding, Y.; Tian, Q.; Zhang, W.; Wang, M.; Zang, Z.; Sun, X.; Li, D.; Si, X.; Li, B. Novel pH sensitivity and colorimetry-enhanced anthocyanin indicator films by chondroitin sulfate co-pigmentation for shrimp freshness monitoring. *Food Control* **2022**, *131*, 108441, https://doi.org/10.1016/j.foodcont.2021.108441.